IEEE Access
Multidisciplinary | Rapid Review | Open Access Journal

Received 26 January 2023, accepted 9 February 2023, date of publication 13 February 2023, date of current version 16 February 2023.

Digital Object Identifier 10.1109/ACCESS.2023.3244408

RESEARCH ARTICLE

Estimation of the Magnetic Signature of Ferromagnetic Nanoparticles by Earth's Magnetic Field

ALEXANDRA C. BARMPATZA, ANARGYROS T. BAKLEZOS, IOANNIS O. VARDIAMBASIS, AND CHRISTOS D. NIKOLOPOULOS

Department of Electronics Engineering, Hellenic Mediterranean University, 73133 Chania, Greece

Corresponding authors: Alexandra C. Barmpatza (abarmpatza@hmu.gr) and Christos D. Nikolopoulos (cnikolo@hmu.gr)

This work was supported in part by the Project "Strengthening and optimizing the operation of MODY services and academic and research units of the Hellenic Mediterranean University," funded by the Public Investment Program of the Greek Ministry of Education and Religious Affairs.

ABSTRACT Envisioning the next generation electrified chemical reactors heated by induction that will be able to provide feedback on the material properties online, allowing early diagnosis of potential problems, authors in this paper study the magnetic behavior of supported cobalt (catalytic) nanoparticles, with both face-centered cubic (fcc) and hexagonal close pack (hcp) crystal structure, when the Earth magnetic field is applied. The investigation and corresponding simulations have been performed with finite element analysis. The *magpar* software has been used, allowing simulation of the hysteresis loop for each ferromagnetic sample. The influence of the next neighbor distance and the impact of the number of the particles on the hysteresis loop are studied. The magnetizations of each cobalt-based sample, along with the hysteresis loop have been calculated by simulations and validated by experiments with satisfactory agreement.. Simulations indicate that the number of the particles (different size, under the same total mass) does not affect the hysteresis loop of the material, while the next neighbor distance, has a significant influence. The objective of the present research paper is to develop a novel, versatile, low cost, in situ method for simulating and evaluating magnetic fields generated from heterogeneous catalysts targeting to real-time remote monitoring diagnostics of the catalytic process.

INDEX TERMS Catalysts, cobalt, finite element method, hysteresis loop, nanoparticles.

I. INTRODUCTION

Magnetic nanoparticles are used in various industrial and medical applications, like the targeted drug delivery, the microelectronics sector, the sensor technology, the high-density memory storage, the heterogeneous catalysis, etc. [1], [2], [3], [4], [5]. Catalytic processes are a vital part of our lives and societies. The presence of catalysts as solids, molecular single-sites, or enzymes allows acceleration of reactions, spanning from life-supporting functions in living micro-organisms to industrial chemical conversions on the megatonne scale. Heterogeneous catalysis with supported nanoparticles is used in the production of a variety of chemicals and by-products [6]. It is worth to mention, that the majority of manmade products (i.e. the 85% of industrial chemical products) pass through at least one catalytic process, 80% of which are catalyzed by solid substances. Especially important processes that support the evolution and convenience of our society are catalyzed by supported ferromagnetic NPs and relevant examples are the synthesis of ammonia, for fertilizer production ensuring the nutrition of a continuously growing population, H2 production, a key future energy carrier but also an important reactant, and the decomposition of pollutants from mobile and static sources, moreover the synthesis of e-fuels from waste feedstocks. Today's main global challenge includes the shift towards sustainable non-fossil-based energy and chemical industry, neutralizing (or ideally reversing) the negative impact of

The associate editor coordinating the review of this manuscript and approving it for publication was Agustin Leobardo Herrera-May.

human activities on the climate. Therefore, there is a need for discoveries, more efficient processes, faster decarbonization, and all the above proceeding at non-linear rates boosting knowledge and technological advancement. Catalysis is a key technology for achieving this goal [7].

Ferromagnetic nanoparticles have found several industrial uses as catalysts and play a pivotal role on specific chemical conversions of high importance, such as the ammonia synthesis and the hydrogen production and utilization. The shape, the size, the composition and the electronic structure of the nanoparticles affects the performance of the catalyst. Furthermore, the properties of modern magnetic materials are strongly influenced by their microstructure [8], [9], [10].

Selwood first defined magnetochemistry as the utilization of magnetic quantities for the solution of chemical problems [11]. The relations of magnetism and chemical bond are the first actual in situ approaches on magnetic measurements in catalysis [12]. A magnetic balance for monitoring the phase changes of iron was also developed in the same period by others [13]. Since the 80s three variations of vibrating sample magnetometer (VSM) were built. Researchers at the Centre National de la recherche Scientifique (CNRS) developed a VSM measuring configuration for performing magnetic studies on catalytic systems at ambient conditions [14]. A VSM instrument based on acoustic oscillations followed [15]. Recently, a VSM design was developed at the department of chemical engineering at the University of Cape Town in collaboration with scientists at Sasol R&T [16]. From the above, it becomes apparent that the small number of operating magnetometers worldwide are based on an outdated measuring principle, The VSM configuration consists of bulky electromagnets, expensive and complicated connections to allow the accommodation of a moving part (vibration of the sample or electromagnet or the sensors). It is worth mentioning that a commercial VSM configuration costs several thousand euro (i.e. 300k€) without modifications for chemical reactor integration. In addition, the signal has low time resolution and cannot be resolved in space. Therefore, this configuration was not adapted widely and, to the best of our knowledge, only the three pre-mentioned VSM configurations to be still in operation. Coil-based sensors [17], optical [18], and atomic magnetometry [19] continuously develop and today simplified sensors can measure magnetic fields in the order of pico Tesla. With the current magnetometer's strength and direction of the magnetic field are resolved accurately. Furthermore, developments in near-field approximation algorithms have allowed the detection of the location of the centre of magnetization [20], [21] while magneto-optic phenomena enable magnetic mapping [22]. Therefore, the intrinsic drawbacks of the utilization of VSM type magnetometers namely the existence of moving parts, low sensitivity, low time resolution, an assumption on the centre of magnetization could be bypassed through the development and utilization of hybrid combinations of coiled magnetometers and magneto-optical devices.

In this study, the magnetic behavior of ferromagnetic nanoparticles under the Earth's magnetic field, is studied targeting to the isolation and measurement of magnetic fields of low intensity from catalytic reactors. Cobalt (Co) nanoparticles with face-centered cubic (fcc) and hexagonal close pack (hcp) structure are investigated, while the simulation is performed using the Finite Element Method (FEM). The simulation results are validated through comparisons with experimental tests. More specifically, two parameters are investigated with respect to their effect on the hysteresis loop: (i) the distance between the particles and (ii) the number of particles under the same mass properties. In each case, the corresponding hysteresis loops are compared.

Driven by the advances in ultra-sensitive magnetic sensors, signal processing, and the developments in operando catalyst characterization our overall objective is to create a novel, simplified and versatile hybrid array of magnetometers, in order to allow monitoring of magnetic fields produced by functional catalytic materials under their working conditions; without any compromise in the reactor plug-flow configuration. For this reason, and as a proof-of-concept, a measuring setup is developed with arrays of coil-based (Fluxgate) magnetometers to measure the magnetic properties of a working catalytic material. Magnetic fields are phase and size-dependent, therefore are hiding valuable information on the state of the catalyst under working conditions.

II. THE INVESTIGATED MATERIALS

The investigated ferromagnetic catalytic materials are Cobalt with fcc and hcp crystal structure respectively. Each model has been created and meshed using GiD software, while the analysis and the post processing have been performed using the *magpar* software [23]. GiD can create the finite element mesh of a geometry and export it in inp format. Then, for the micromagnetic modelling, the Finite Element Method (FEM) module of the *magpar* code was applied. The choice of the *magpar* software was done because is applicable in both cases of uniaxial and cubic anisotropy, uses the FEM while the majority of existing commercial and open source micromagnetics programs use the finite difference method and it is also versate because includes static energy minimization and dynamic time integration methods. The FEM is a well-known method, which can simulate and solve electromagnetic problems with satisfying accuracy in various fields of computer aided engineering, like structural analysis, fluid dynamics, electromagnetic field computation, as well as micromagnetics [23].

The properties of each sample are summarized in Table 1. In order to represent the two different crystal structures in the *magpar*.krn file, the magneto-crystalline anisotropy constant is set to $K = 2.7 \times 10^5$ J/m^3 and 4.5×10^5 J/m^3, for the fcc and the hcp morphology respectively, while the exchange constant for both cases is taken equal to $A = 1.3 \times 10^{-11}$ J/m [8], [9]. The used meshing topology is a simple quadratic mesh, while the number of tetrahedral elements varies from

TABLE 1. Properties of the two studied nanoparticles samples.

	FCC-Co	HCP-Co
Sample Weight	11.19 g	0.076 g
Embedded in	Wax	Carbon
Co	20% wt	20% wt
DOR	80%	99%
Structure	FCC	HCP
M_S	168 emu/g	150 emu/g

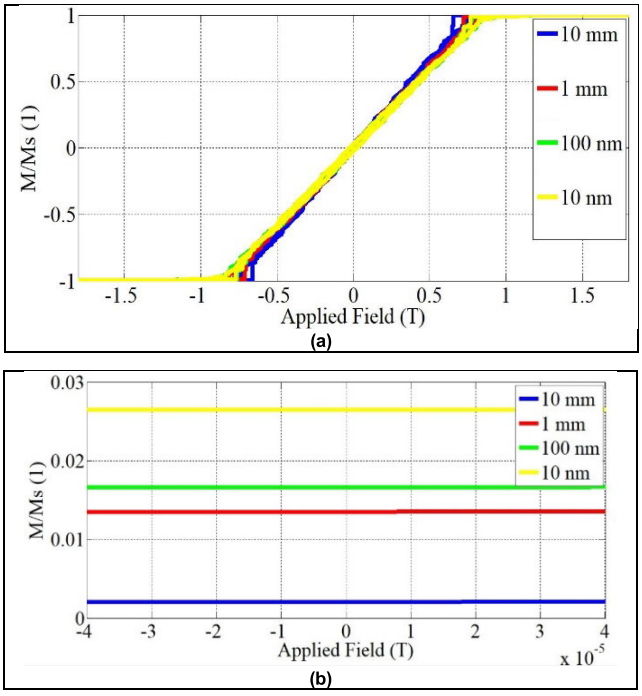

FIGURE 1. Hysteresis loops of the fcc-Co for two spheres with distances 10 mm, 1 mm, 100 nm and 10 nm, as a function of the applied field. (a) Full hysteresis loops. (b) Focused hysteresis loops.

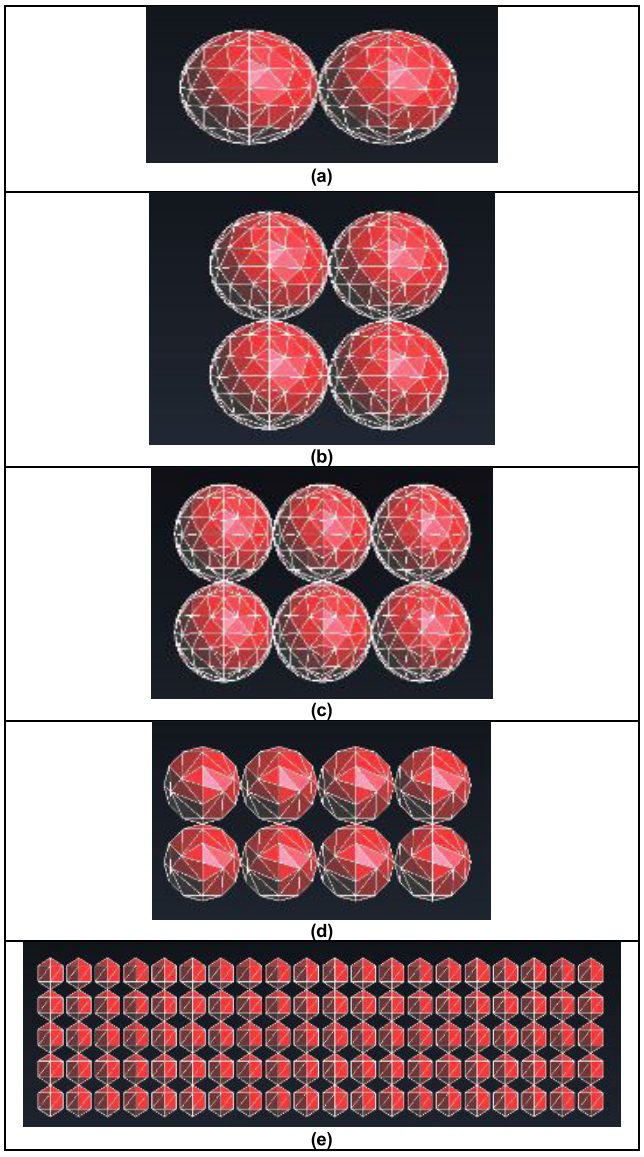

FIGURE 2. The simulated approximate meshed model of the catalyst with (a) two, (b) four, (c) six, (d) eight, and (e) one hundred spheres.

350 until 1600 depending on the spheres number. The average convergence time, in order one full loop to be simulated, is 48 hours.

III. SIMULATION RESULTS – FCC-Co

At first, authors performed two different simulations for sample A. In the first case, the total volume of the material was simulated by two equivalent spheres located in different distances, and the effect of their distance was studied. In the second case, the catalyst was simulated by different number of spheres (always with the same total mass value) and the influence of the number of spheres in the hysteresis loop of the catalyst was examined.

A. DEPENDENCE ON THE DISTANCE BETWEEN THE PARTICLES

In this section, the dependence from the distance between the cobalt particles is investigated. In all studied cases, two spheres with four different distances between them are simulated. These two spheres cover the total number of the sample nanoparticles, with an equivalent radius of each sphere taken equal to 2.885 mm. The calculation of the radius of each sphere is achieved using the Cobalt density, which is equal to 8900 kg/m^3 for the half of the total mass for each sphere. The distances of 10 mm, 1 mm, 100 nm and 10 nm are chosen for investigation purposes. Fig. 1 presents the hysteresis loops for the four simulation cases. From Fig. 1(b), when the hysteresis loop is focused in the range of Earth's magnetic field ($\sim 4 \times 10^{-5}$ T), it is obvious that the distance between the particles affects the hysteresis loop of fcc Cobalt. Fig. 1 depicts that the magnetization (in the presence of the Earth's magnetic field) is reduced, when the distance between the particles increases.

B. DEPENDENCE ON THE PARTICLE NUMBER

In this paragraph, the effect of the number of particles on the hysteresis loop is presented. As shown in Fig.2, the catalyst is simulated with five different ways: (i) as two spheres with radii equal to the average radius of the real material, (ii) as four spheres, (iii) as six spheres, (iv) as eight spheres and (v) as one hundred spheres. In fact, two, four, six, eight or one hundred equivalent spheres are simulated respectively, with their volume covering every time the total number of the sample nanoparticle. The radius of each sphere depicted in Fig. 2(a) is 2.885 mm, in Fig. 2(b) is 2.2898 mm, in Fig. 2(c) is 2.0004 mm, in Fig. 2(d) is 1.8174 mm and in Fig. 2(e) is 0.78311 mm. The distance between particles is 10 nm in all simulated cases.

Fig. 3 presents the hysteresis loops for the five simulated cases, and the slight effect of the number of spheres (under the same total mass) on the hysteresis loop of the fcc-Co material. Fig. 3(b) shows that the magnetization of the catalytic material, when the Earth's magnetic field is present (applied as external field), is approximately 0.028 times the saturation magnetization M_S. The small numerical deviations are a result of different used meshes, between the simulations, imposed by the different number of simulated spheres.

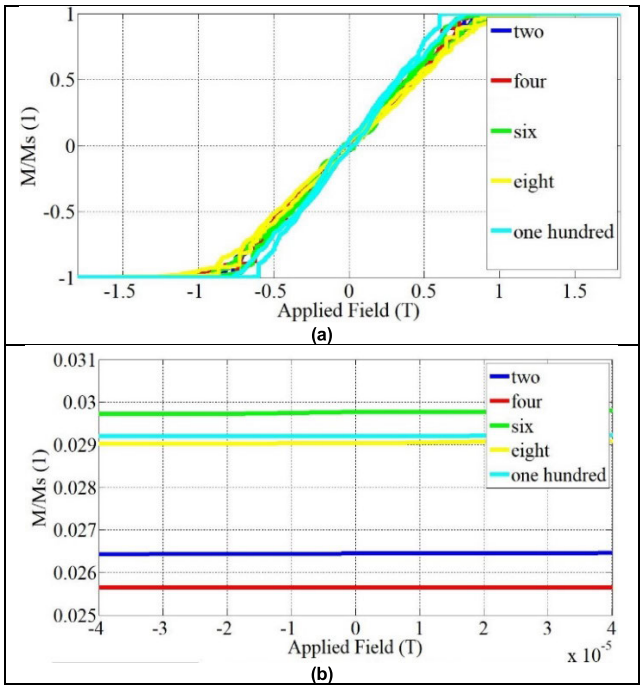

FIGURE 3. Hysteresis loops of the fcc-Co as a function of the applied field, when the material is simulated using two, four, six, eight and one hundred spheres. (a) Full hysteresis loop. (b) Focused hysteresis loop.

Fig. 3(b) focusses on the part of the hysteresis loop that correspond to the Earth's applied magnetic field, since this is the value that authors try to validate the methodology. Consequently, the magnetization for the 40 × 10-6 T applied Earth's field is about equal to 4.7 emu/g. As it can be seen the number of simulated spheres has almost no effect on the hysteresis loop.

IV. SIMULATION RESULTS – HCP-Co

In this section, hcp-Co, whose properties are also described in Table 1, is simulated. Since the previous analysis revealed that the number of the simulated spheres has almost no effect on the hysteresis loop of the ferromagnetic nanoparticles, in this case the material is simulated using only one sphere. The radius of this sphere is calculated like before for fcc-Co, taking into account the Co density as equal to 8900 kg/m^3 for the total mass of the sample. Consequently, the value of the radius is 0.73904 mm, and the results are depicted in Fig. 4. Fig. 4(b) focusses on the part of the hysteresis loop that corresponds to the Earth's applied magnetic field in the hcp-Co, thus the magnetization is approximately 0.007 times the saturation magnetization of the material, resulting on a value of 1.05 emu/g. It can be easily observed that the moment value per mass exhibits divergence between the hysteresis loop of the fcc-Co sample (4.7 emu/g), and the hcp-Co sample (1.05 emu/g) due to the strong perpendicular anisotropy effect [8].

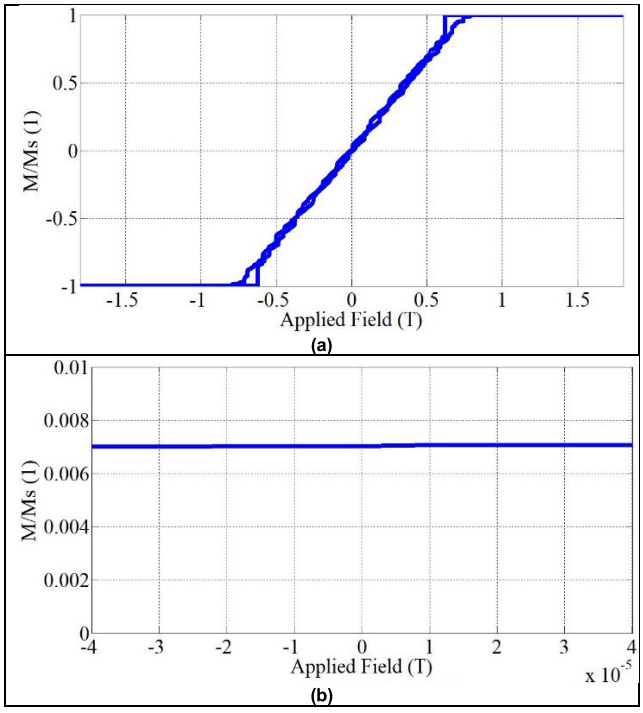

FIGURE 4. Hysteresis loop of the hcp-Co as a function of the applied field, when the material is simulated using one sphere with radius the average radius of the material. (a) Full hysteresis loop. (b) Focused hysteresis loop.

V. MAGNETIC MOMENT ESTIMATION VIA HEURISTIC APPROACH

The magnetic field of the nanometer-sized particles for each Sample Under Test (SUT) can be represented by a magnetic dipole. Assuming that $\boldsymbol{R}_{dipole}\,(x, y, z)$ is the position vector of the dipole source, $\boldsymbol{m}$ is the moment vector of the dipole and

$\boldsymbol{R}_k$ is the position vector of an observation point K as depicted in Fig. 5, the magnetic field is expressed as [24]:

$$\boldsymbol{B}(\boldsymbol{n}, t) = \frac{\mu_0}{4\pi}[3\boldsymbol{n}(\boldsymbol{n}\cdot\boldsymbol{m}) - \boldsymbol{m}]\frac{1}{r^3} \tag{1}$$

where $\boldsymbol{r} = \boldsymbol{R}_k - \boldsymbol{R}_{dipole}$, $r = |\boldsymbol{r}|$, and $\boldsymbol{n} = \boldsymbol{r}/r$.

In accordance with this formulation three moment coordinates (m_x, m_y, m_z) are allocated to the dipole source. The magnetic field components at a random point with coordinates $\boldsymbol{R}_k\,(x_k, y_k, z_k)$ as depicted in Fig. 5, can be calculated by:

$$\begin{aligned} B_x &= \frac{\mu_o}{4\pi}\left[\frac{3\,(x_k - x)\cdot C}{r^5} - \frac{m_x}{r^3}\right] \\ B_y &= \frac{\mu_o}{4\pi}\left[\frac{3\,(y_k - y)\cdot C}{r^5} - \frac{m_y}{r^3}\right] \\ B_z &= \frac{\mu_o}{4\pi}\left[\frac{3\,(z_k - z)\cdot C}{r^5} - \frac{m_z}{r^3}\right] \end{aligned} \tag{2}$$

where $C = m_x\,(x_k - x) + m_y\,(y_k - y) + m_z\,(z_k - z)$ and $r = \sqrt{(x_k - x)^2 + (y_k - y)^2 + (z_k - z)^2}$.

The total magnitude of the magnetic field from a single dipole is:

$$|B_{total}| = \sqrt{B_x^2 + B_y^2 + B_z^2} \tag{3}$$

It should be noted that in our case the sample's mass center (geometrical center of the volume) is considered as the center of the measurement facility's coordinate system simplifying equation (2).

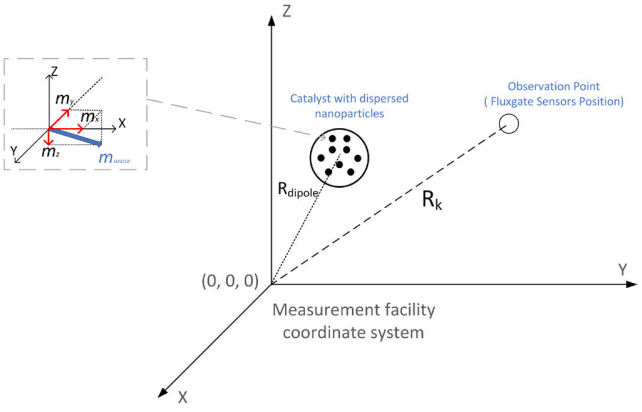

FIGURE 5. Formulation of the magnetic dipole source characterization problem.

The magnetic field vector is expressed by its components since the measuring fluxgate sensors typically provide precision measurements of static and alternating magnetic fields in three axes (B_x, B_y, B_z). However, several types of sensors measure the amplitude of the magnetic field as given by (3).

VI. INVERSE ELECTROMAGNETIC SCATTERING PROBLEM

In order to acquire the magnetic properties of the ferromagnetic catalytic nanoparticle sample, under the homogeneous magnetic field of the Earth, two independent measurements should be performed almost simultaneously. The total magnetic field at the fluxgate sensor $B_{xTotal}\,(t)$, is formulated as:

$$B_{x_{Total}}(t) = B_{x_{sample}}(t) + B_{x_{noise}}(t) \tag{4}$$

considering the various sources of magnetic noise (such as the Earth's magnetic field, the power line interference, etc.).

In order to measure $B_{xsample}\,(t)$ properly, the first measurement is performed without the ferromagnetic sample, and immediately after the second measurement follows with the sample present. Since the powder catalytic sample has the smallest dimension in the overall system, the sample can be represented by an infinitesimal magnetic dipole placed at the origin of the coordinate system of the measurement setup. Catalysts have been prepared by the exact incipient wetness impregnation recipe exhibit the characteristics presented in [25] and [26]. Under this assumption, since the nanoparticle have identical characteristics, the infinitesimal source has a moment equal to the average magnetic moment of the various magnetic sources of the sample. This equivalent moment can be extracted exploiting the aforementioned measurement with the use of a heuristic methodology, such as the Differential Evolution (DE) algorithm [27], [28], [29], [30]. The source characterization when the measured magnetic field values are given, poses an inverse problem. Considering that the sample's location is at the origin ($x_{sample} = 0$, $y_{sample} = 0$, $z_{sample} = 0$) and employing equations (2) – (3), only one measurement is necessary in order to estimate the magnetic moment of the equivalent dipole source. The heuristic methodology assigns iteratively values to the dipole's magnetic moments in order to minimize at the sensor locations the difference between the produced magnetic field (from the equivalent source) and the measured $B_{xSample}\,(t)$. For validation purposes another identical fluxgate magnetometer is placed at the opposite direction of the first, symmetrically along the x- axis.

VII. EXPERIMENTAL RESULTS

The simulation results are tested and validated through comparisons with experimental results. The experiments were conducted at the Telecommunications & Electromagnetic Applications Laboratory of the Electronic Engineering Department of the Hellenic Mediterranean University. Fig. 6(a) depicts the full experimental set up with two fluxgate magnetometers and the vial with the ferromagnetic sample present, while Figs. 6b and 6c show the two magnetometers used with each of the A and B samples respectively.

A. FCC-CO

At first, experiments for the first sample were conducted, as depicted in Fig. 6(b). Figs. 7(a), 7(b) and 7(c) present the magnetic field versus time, measured by magnetometers 1 and 2, in x-, y- and z- axes respectively, when only the magnetic field of the Earth is measured. This measurement precedes the one of Fig. 9, where the fcc-Co is present on the acquisition process.

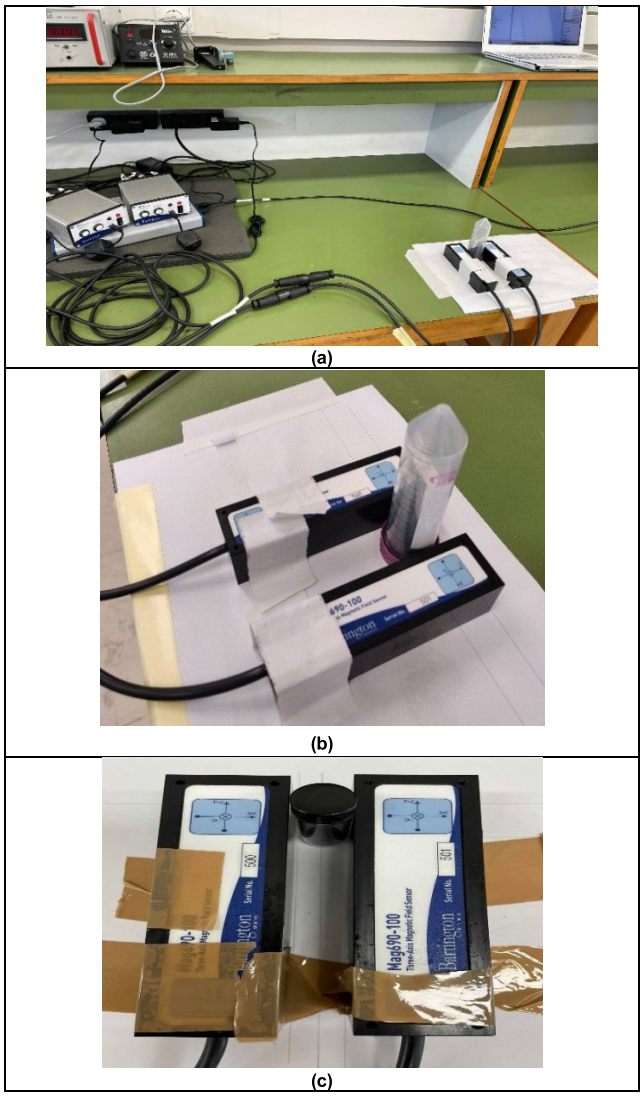

FIGURE 6. The experimental set up. (a) The full experimental set up which consists of the two magnetometers, the sample and the computer connected to LabVIEW. (b) The fcc-Co sample with the two magnetometers. (c) The hcp-Co sample with the two magnetometers.

Fig. 8 shows the total magnetic field amplitude of the Earth versus time that give the magnetometers 1 and 2.

Accordingly, Figs. 9(a), 9(b) and 9(c) depict the magnetic field captured in the x-, y- and z- axes, when the ferromagnetic sample of the fcc-Co is present.

The amplitude of the total magnetic field, derived from the three axes when the catalyst is present, is depicted in Fig.10. More specifically, Fig. 10(a) presents the measurement from magnetometer 1, while Fig. 10(b) the measurement from magnetometer 2 (which is a second independent measurement for verification purposes).

Subtracting the magnetic field values presented in the Fig. 9 with the magnetic field values presented in the Fig. 7 and using the EDE algorithm, we can export the magnetization in axes x, y and z, when the magnetic field of the Earth is applied in the fcc-Co sample. The procedure can be

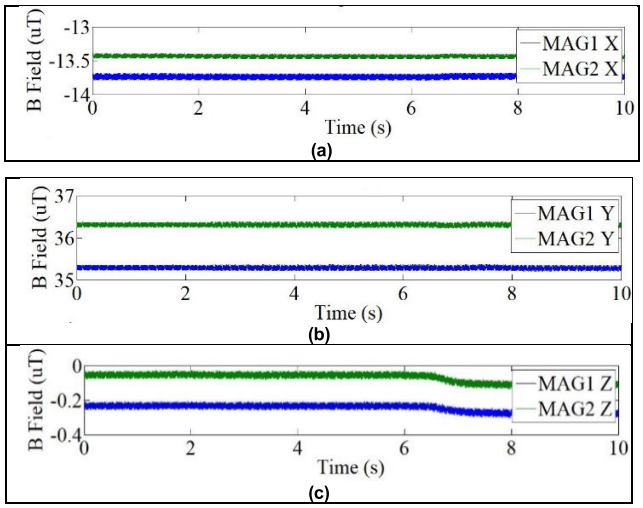

FIGURE 7. Ambient magnetic field vector from the two magnetometers (MAG1-magnetometer 1, MAG2-magnetometer 2).

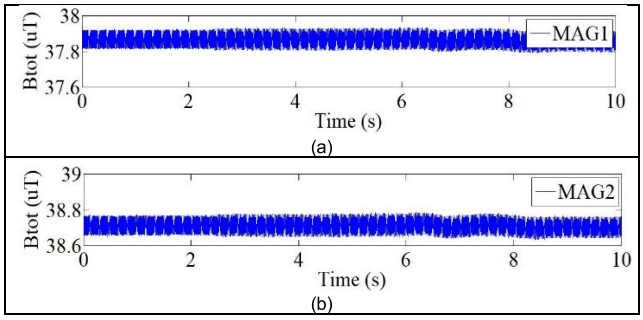

FIGURE 8. Ambient magnetic field magnitude during measurement (a) magnetometer 1 and (b) magnetometer 2.

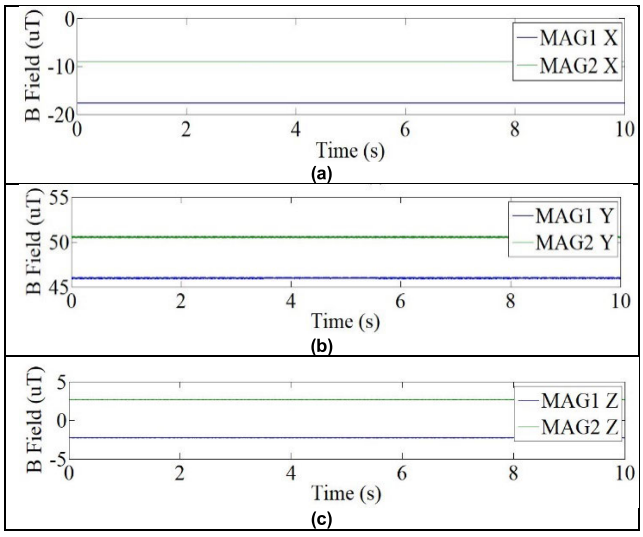

FIGURE 9. fcc-Co sample magnetic field vector measurement under the Earth's magnetic field (a) the x-axis, (b) the y-axis, and (c) the z-axis (MAG1-magnetometer 1, MAG2-magnetometer 2).

achieved for both magnetometers, and the values of the first magnetometer can be used for results validation of the second magnetometer.

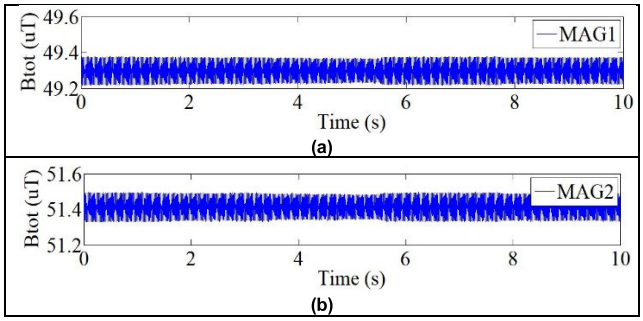

FIGURE 10. fcc-Co sample magnetic field magnitude measurement (a) magnetometer 1, and (b) magnetometer 2.

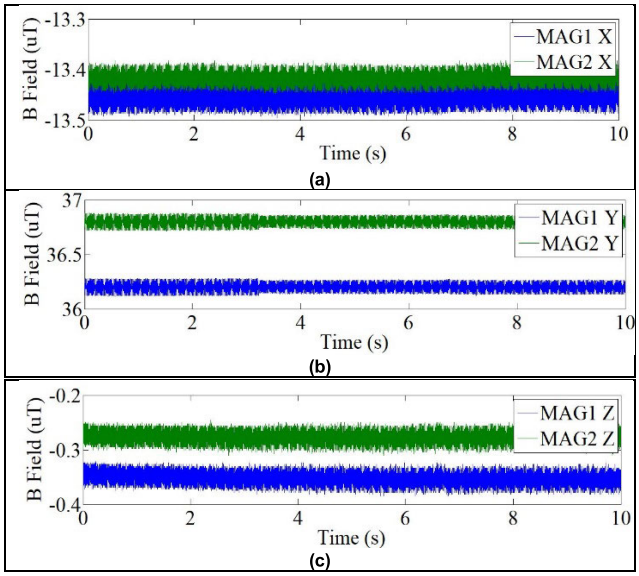

FIGURE 11. Ambient magnetic field vector from the two magnetometers (MAG1-magnetometer 1, MAG2-magnetometer 2).

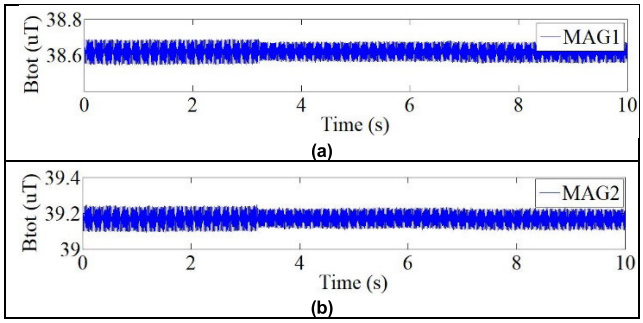

FIGURE 12. Ambient magnetic field magnitude during measurement (a) magnetometer 1 and (b) magnetometer 2.

Consequently, the magnetization derived from the experimental procedure is about 4.4 emu/g, when $B_x = -3.9083 \times 10^{-6}$ T, $B_y = -2.0046 \times 10^{-6}$ T and $B_z = -10.6902 \times 10^{-6}$ T, for a measurement point at distance x = −0.038 m, y = 0 m and z = 0.015 m from the sample. This experimental result is pretty close with the one from the simulation procedure (4.7 emu/g), and therefore it can validate the simulation.

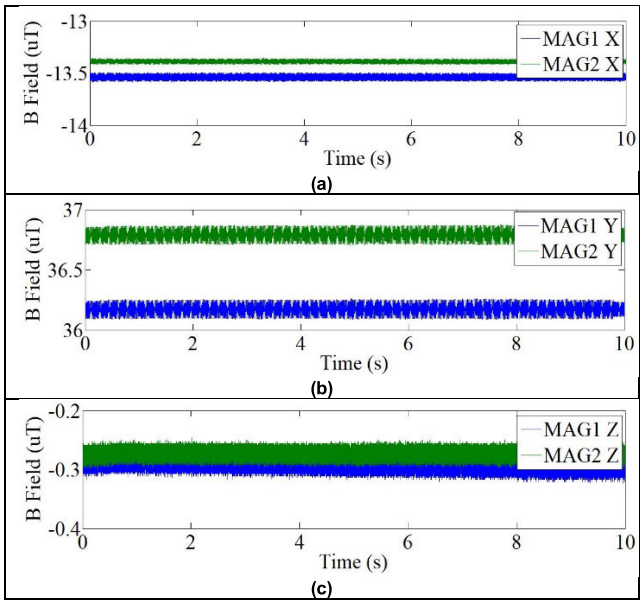

FIGURE 13. hcp-Co sample magnetic field vector measurement under the Earth's magnetic field (a) the x-axis, (b) the y-axis, and (c) the z-axis (MAG1-magnetometer 1, MAG2-magnetometer 2).

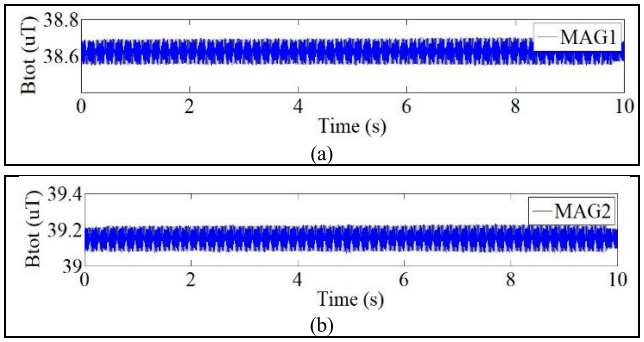

FIGURE 14. hcp-Co sample magnetic field amplitude measurement under the Earth's magnetic field, (a) magnetometer 1, and (b) magnetometer 2.

B. HCP-CO

Secondly, the measurements have been done, using the same method, for the hcp-Co. Fig. 11a, 11b and 11c depict the Earth magnetic field, derived by magnetometers 1 and 2, in axes x, y and z respectively, while Fig. 12 shows the total Earth magnetic field that give the magnetometers 1 and 2.

Accordingly, Figs. 13(a), 13(b) and 13(c) show the Earth's magnetic field enhanced by the magnetic field of the hcp-Co sample in the x-, y- and z- axes, which give the magnetometers 1 and 2. The total magnetic field, from the three axes, is depicted in Fig. 14.

Following the same procedure as before for the fcc-Co sample, and taking into consideration the measurements, for $B_x = -0.0929 \times 10^{-6}$ T, $B_y = 0.0585 \times 10^{-6}$ T and $B_z = 0.0284 \times 10^{-6}$ T and for a measurement point at distance x=-0.0235 m, y=0 m and z=0.015 m from the sample, the magnetization is found equal to 0.95 emu/g. This value can validate the corresponding simulation results (1.05 emu/g).

VIII. CONCLUSION

In this article, the magnetic behavior of Co-based catalytic materials, under the effect of the Earth magnetic field, is studied. More specifically, two Co-based materials are investigated, one with predominantly fcc crystal structure and another with hcp crystal structure. The *magpar* software is used for the FEM simulations and the hysteresis loop exported for each case. The influence (i) of the distance between the particles and (ii) of their number, on the material hysteresis loop, is studied for the first sample. At first, the catalyst is simulated as two spheres with different distances among them and the dependence of the distance is taken into account. Subsequently, the same quantity of material is simulated with a varying number of spheres, in order to examine the dependence from the number of particles.

The analysis reveals that increasing the distance between the particles causes the sample magnetization to decrease. On the other hand, the number of particles does not affect the hysteresis loop of the material. Comparing the two crystal structures (fcc and hcp), different magnetic behavior can be observed due to the catalytic role of the magnetocrystalline anisotropy. The magnetic moment value per mass for fcc-Co (4.7 emu/g) is higher, compared to the corresponding value of hcp-Co (1.05 emu/g). It should be noted that simulation and experimental results exhibit good agreement, regarding the induced magnetization under the Earth's magnetic field for both the available samples.

This study is the first step of a project which aims to create a novel and complete measurement system, based in magnetometers, for operando catalyst characterization. As it can be seen from the findings, the hysteresis loop and consequently the magnetic moment, are influenced by the kind of nanoparticle, its crystal structure, the dimensions of the nanoparticles and the distance between them. Taking advantage of phase information and various details about catalyst in situ, industries can exploit these novel techniques and develop more robust and sustainable chemical processes. Thus, future work under the same direction would be the implementation of a measuring setup able to provide different values in the external applied field to cover the complete hysteresis loop. Concluding, the better understanding of catalysis science by state-of-the-art tools is one of the core businesses of various industries and research institutes.

ACKNOWLEDGMENT

The authors would like to thank Dr. Nikolaos Tsakoumis, Researcher with the Kinetics and Catalysis Group, SINTEF Industry, Norway, for providing the cobalt nanoparticle samples and his insight and fruitful comments.

REFERENCES

[1] A. Ali, T. Shah, R. Ullah, P. Zhou, M. Guo, M. Ovais, Z. Tan, and Y. Rui, "Review on recent progress in magnetic nanoparticles: Synthesis, characterization, and diverse applications," *Frontiers Chem.*, vol. 9, Jul. 2021, Art. no. 629054.

[2] E. M. Materón, C. M. Miyazaki, O. Carra, N. Joshi, P. H. S. Picciani, C. J. Dalmaschio, F. Davis, and F. M. Shimizu, "Magnetic nanoparticles in biomedical applications: A review," *Appl. Surf. Sci. Adv.*, vol. 6, Dec. 2021, Art. no. 100163.

[3] A. Akbarzadeh, M. Samiei, and S. Davaran, "Magnetic nanoparticles: Preparation, physical properties, and applications in biomedicine," *Nanosc. Res. Lett.*, vol. 7, no. 1, pp. 1–13, Feb. 2012.

[4] A. A. El-Gendy, M. Qian, Z. J. Huba, S. N. Khanna, and E. E. Carpenter, "Enhanced magnetic anisotropy in cobalt-carbide nanoparticles," *Appl. Phys. Lett.*, vol. 104, no. 2, Jan. 2014, Art. no. 023111.

[5] N. Tsakoumis, A. T. Baklezos, I. O. Vardiambasis, T. N. Kapetanakis, and C. D. Nikolopoulos, "Fluxgate configuration for obtaining magnetic properties of catalytic nanoparticles: A feasibility study," in *Proc. IEEE Int. Instrum. Meas. Technol. Conf. (I2MTC)*, May 2020, pp. 1–5.

[6] S. Schauermann, N. Nilius, S. Shaikhutdinov, and H.-J. Freund, "Nanoparticles for heterogeneous catalysis: New mechanistic insights," *Accounts Chem. Res.*, vol. 46, no. 8, pp. 1673–1681, Dec. 2012.

[7] N. E. Tsakoumis, A. P. E. York, D. Chen, and M. Rønning, "Catalyst characterisation techniques and reaction cells operating at realistic conditions; towards acquisition of kinetically relevant information," *Catal. Sci. Technol.*, vol. 5, pp. 4859–4884, Jul. 2015.

[8] L. G. Vivas, R. Yanes, O. Chubykalo-Fesenko, and M. Vazquez, "Coercivity of ordered arrays of magnetic Co nanowires with controlled variable lengths," *Appl. Phys. Lett.*, vol. 98, no. 23, Jun. 2011, Art. no. 232507.

[9] C. Bran, Y. P. Ivanov, D. G. Trabada, J. Tomkowicz, R. P. del Real, O. Chubykalo-Fesenko, and M. Vazquez, "Structural dependence of magnetic properties in co-based nanowires: Experiments and micromagnetic simulations," *IEEE Trans. Magn.*, vol. 49, no. 8, pp. 4491–4497, Aug. 2013.

[10] S. Shalini, "Structural and magnetic properties of epitaxial rare-Earth cobalt thin films," Ph.D. dissertation, Mater. Earth Sciences Dept., Technische Universitat Darmstadt, Darmstadt, Germany, 2020.

[11] P. W. Selwood, *Magnetochemistry*. New York, NY, USA: Interscience, 1943.

[12] P. W. Selwood, "The mechanism of chemisorption: Hydrogen on Nickel. I," *J. Amer. Chem. Soc.*, vol. 78, no. 16, pp. 3893–3897, Aug. 1956, doi: 10.1021/ja01597a009.

[13] L. J. E. Hofer and E. W. Toor, "Magnetic balance for ferromagnetism," *Rev. Sci. Instrum.*, vol. 33, no. 4, pp. 417–422, Apr. 1962, doi: 10.1063/1.1717868.

[14] A. Dalmon, *Magnetic Measurements and Catalysis–Catalyst Characterization: Physical Techniques for Solid Materials*, B. Imelik J. C. Vedrine, Eds. Boston, MA, USA: Springer, 1994, pp. 585–609, doi: 10.1007/978-1-4757-9589-9_21.

[15] P. A. Chernavskii, G. V. Pankina, and V. V. Lunin, "Magnetometric methods of investigation of supported catalysts," *Russian Chem. Rev.*, vol. 80, no. 6, pp. 579–604, Jun. 2011, doi: 10.1070/RC2011v080n06ABEH004187.

[16] M. Claeys, E. W. J. van Steen, J. L. Visagie, and J. van de Loosdrecht, "Magnetometer," U.S. Patent 8 773 118 B2, 2014.

[17] J. Luomahaara, V. Vesterinen, L. Grönberg, and J. Hassel, "Kinetic inductance magnetometer," *Nature Commun.*, vol. 5, no. 1, pp. 1–7, Sep. 2014, doi: 10.1038/ncomms5872.

[18] M. Tatarakis, "Measuring huge magnetic fields," *Nature*, vol. 415, p. 280, Jan. 2002, doi: 10.1038/415280a.

[19] I. K. Kominis, T. W. Kornack, J. C. Allred, and M. V. Romalis, "A subfemtotesla multichannel atomic magnetometer," *Nature*, vol. 422, pp. 596–599, Apr. 2003, doi: 10.1038/nature01484.

[20] A. Junge and F. Marliani, "Prediction of DC magnetic fields for magnetic cleanliness on spacecraft," in *Proc. IEEE Int. Symp. Electromagn. Compat.*, Aug. 2011, pp. 834–839, doi: 10.1109/ISEMC.2011.6038424.

[21] C. D. Nikolopoulos, A. T. Baklezos, and C. N. Capsalis, "On achieving spacecraft level magnetic cleanliness with proper equipment ordinance of DC and ELF magnetic sources," *IEEE Trans. Electromagn. Compat.*, vol. 62, no. 6, pp. 2714–2724, Dec. 2020, doi: 10.1109/TEMC.2020.2992682.

[22] N. Akai and K. Ozaki, "3D magnetic field mapping in large-scale indoor environment using measurement robot and Gaussian processes," in *Proc. Int. Conf. Indoor Positioning Indoor Navigat. (IPIN)*, Sep. 2017, pp. 1–7, doi: 10.1109/IPIN.2017.8115960.

[23] W. Scholz, "Scalable parallel micromagnetic solvers for magnetic nanostructures," *Comput. Mater. Sci.*, vol. 28, no. 2, pp. 366–383, Oct. 2003.

[24] J. Jackson, *Classical Electrodynamics*, 1st ed. New York, NY, USA: Wiley, 1962.

[25] N. E. Tsakoumis, R. Dehghan-Niri, M. Rønning, J. C. Walmsley, Ø. Borg, E. Rytter, and A. Holmen, "X-ray absorption, X-ray diffraction and electron microscopy study of spent cobalt based catalyst in semi-commercial scale Fischer–Tropsch synthesis," *Appl. Catal. A, Gen.*, vol. 479, pp. 59–69, Jun. 2014, doi: 10.1016/j.apcata.2014.03.035.
[26] N. E. Tsakoumis, A. Voronov, M. Rønning, W. V. Beek, Ø. Borg, E. Rytter, and A. Holmen, "Fischer–Tropsch synthesis: An XAS/XRPD combined in situ study from catalyst activation to deactivation," *J. Catal.*, vol. 291, pp. 138–148, Jul. 2012, doi: 10.1016/j.jcat.2012.04.018.
[27] R. Storn and K. Price, "Differential evolution—A simple and efficient adaptive scheme for global optimization over continuous spaces," Berkley, Greenwich, CT, USA, Tech. Rep. TR-95-012, 1995.
[28] D. Dawar and S. Ludwig, "Differential evolution with dither and annealed scale factor," in *Proc. IEEE Symp. Differ. Evol. (SDE)*, Dec. 2014, pp. 1–8, doi: 10.1109/SDE.2014.7031528.
[29] P. Kumar and M. Pant, "Enhanced mutation strategy for differential evolution," in *Proc. IEEE Congr. Evol. Comput.*, Jun. 2012, pp. 1–6, doi: 10.1109/CEC.2012.6252914.
[30] A. T. Baklezos, "Steady state emissions modeling of low frequency magnetic and electric fields generated by GOCE CDMU," in *Proc. ESA Workshop Aerosp. EMC (Aerospace EMC)*, May 2019, pp. 1–5, doi: 10.23919/AeroEMC.2019.8788927.

ALEXANDRA C. BARMPATZA was born in Athens, Greece, in March 1991. She received the Diploma degree in electrical and computer engineering and the Ph.D. degree in electrical machines condition monitoring and fault diagnosis from the University of Patras, Patras, Greece, in 2013 and 2021, respectively. She is currently a Postdoctoral Research Fellow in the electromagnetism with the Department of Electronic Engineering, Hellenic Mediterranean University, Crete, Greece. Her research interests include designing with FEM, electromagnetism, electrical machine designing, power electronics, machine faults, and loss analysis. She serves as a Reviewer for IEEE TRANSACTIONS and other scientific journals.

ANARGYROS T. BAKLEZOS was born in Lamia, Greece, in 1981. He received the B.S. and M.Sc. degrees in physics and telecommunication engineering from the National and Kapodistrian University of Athens (UOA), in 2008 and 2014, respectively, and the Ph.D. degree from the National Technical University of Athens (NTUA), in 2020.

He is currently an Adjunct Lecturer with the Department of Electronic Engineering, Hellenic Mediterranean University (HMU), and a Researcher with the School of Electrical and Computer Engineering, NTUA. His research interests include the field of electromagnetic compatibility, inverse scattering problems, electromagnetic field modeling for space applications and EM cleanliness, and antenna design for radiometry applications.

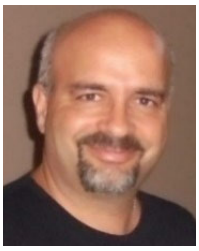

IOANNIS O. VARDIAMBASIS received the Diploma degree in electrical engineering and the Ph.D. degree in electrical and computer engineering from the National Technical University of Athens (NTUA), Greece.

He is currently a Professor in microwave communications, the Director of the Division of Telecommunications, the Director of the Telecommunications and Electromagnetic Applications Laboratory, and the Director of the Master's program in "Telecommunication and Automation Systems" with the Department of Electronic Engineering, Hellenic Mediterranean University (HMU). His research interests include antennas, waveguides, microwave technology and applications, electromagnetic wave propagation, radiation and scattering, biological effects of electromagnetic fields, wearable technology, boundary value problems, wireless communications, sensors networks, neural networks, and artificial intelligence.

CHRISTOS D. NIKOLOPOULOS was born in Athens, Greece, in 1981. He received the B.S. and M.Sc. degrees in physics and telecommunication engineering from the National and Kapodistrian University of Athens (UOA), in 2006 and 2011, respectively, and the Ph.D. degree from the National Technical University of Athens (NTUA), in 2014.

He is currently an Assistant Professor with the Department of Electronic Engineering, Hellenic Mediterranean University (HMU), in addition to his long-standing affiliation as a Research Associate with the Wireless and Long-Distance Communication Laboratory, Department of Electrical and Computer Engineering, NTUA. His research interests include the field of electromagnetic compatibility, inverse electromagnetic scattering problems, magnetic cleanliness, antenna design, and propagation. His recent research focuses on modeling and measuring techniques of electromagnetic emissions from space mission's equipment.